Magnetic Shape Sensing of a Continuum Robot Segment

Soham Sachin Purohit
Indian Institute of Technology Bombay
Mumbai, India

Cameron Forbrigger
University of Toronto
Toronto, Canada

Changyan He
University of Toronto
Toronto, Canada

(Dated: May 2022-July 2022)

Continuum robots have wide applicability in the medical field, due to their ability to form a variety of shapes. With this, comes a need to have the ability to remotely detect the shape assumed by the robot. The goal of this project was to demonstrate the shape sensing of continuum robots over large deflections using an embedded permanent magnet-based shape sensing system. A design methodology was developed for integrating magnetic sensors and permanent magnet material in a continuum robot to ensure a good signal-to-noise ratio for the field measurements. A single-segment continuum robot was fabricated and a shape sensing algorithm was implemented. The performance of the shape-sensing algorithm was evaluated experimentally.

I. INTRODUCTION

Continuum robots offer compelling advantages over conventional rigid-link robots in biomedical applications, such as their ability to navigate narrow and tortuous passages and improved safety due to their mechanical compliance. However, accurately controlling continuum robots is a major challenge due to the difficulty in determining their shape in real time. A recent survey paper [1] evaluated a variety of shape sensing/estimation methods that have been developed for continuum robots. One such method is permanent magnet (PM)-based shape sensing, where magnetic field measurements are used to estimate the pose of embedded magnetic material in the continuum robot body. Like other position-based sensor methods, PM-based shape sensing operates without exposing patients to ionizing radiation, can operate without direct line-of-sight to the robot, and can operate over large deflections. However, unlike inertial measurement unit (IMU)-based or electromagnetic (EM)-based tracking approaches, PM-based shape sensing is not subject to drift problems and does not necessarily require external sensor arrays [1]. As shown by [2] and illustrated in Fig. 1, magnetic sensors and magnetic material can both be embedded in a robot to determine its shape without an external sensor array, thereby potentially reducing the complexity and cost of the robot. However, this approach lacked the magnetic modelling necessary for accurate results in large deflections.

The objective of this project was to demonstrate the shape sensing of a constant curvature, single-segment, centimeter-scale, continuum robot over large deflections using an embedded permanent magnet-based shape sensing system. Fig. 1 displays a simplistic representation of the embedded shape sensing system. A design methodology was developed for integrating magnetic sensors and permanent magnet material in a continuum robot to ensure a good signal-to-noise ratio for the field measurements. A single-segment continuum robot was fabricated

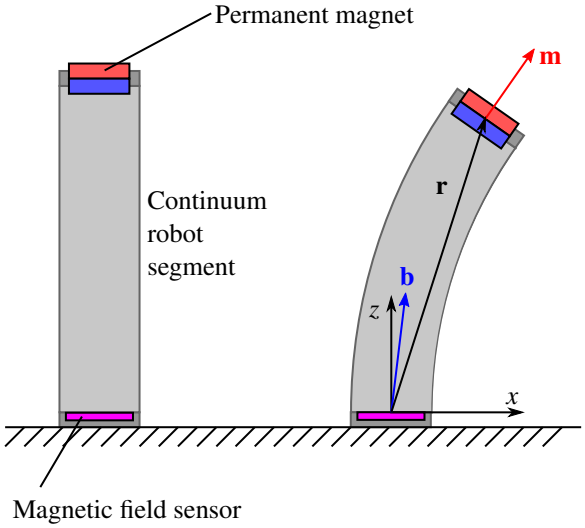

FIG. 1: An illustration of the embedded PM-based shape sensing system in a single continuum robot segment. The field sensor in the base of the segment measures the magnetic field **b** produced by a permanent magnet at the end of the segment. The field measurement can then be used to estimate the orientation of the magnet **m** and its position **r**.

and a shape sensing algorithm was implemented. An experimental setup was designed along with experiments for calibration and compensation, and the performance of the shape-sensing algorithm was evaluated experimentally.

II. ANALYTICAL MODEL

A conceptual model of the bending segment is depicted in Fig. 2. Assuming constant curvature bending

$$L = \rho\varphi\,, \tag{1}$$

where L is the segment length, ρ is the radius of curvature, and $\varphi \in [0, \pi]$ is the (polar) bending angle of the segment. The bending plane $(x'z)$ is normal to the horizontal (xy) plane, and is at an angle of $\theta \in]-\pi, \pi]$ from the xz plane.

The position vector from the sensor location at the origin to the magnet location at the tip of the segment is $\mathbf{r} = r\hat{\mathbf{r}}$, where

$$\hat{\mathbf{r}} = \begin{bmatrix} \cos\theta \sin(\varphi/2) \\ \sin\theta \sin(\varphi/2) \\ \cos(\varphi/2) \end{bmatrix}\,, \tag{2}$$

is a unit vector and

$$r = 2\rho \sin(\varphi/2)\,, \tag{3}$$

is the distance (chord length) from the magnet to the sensor.

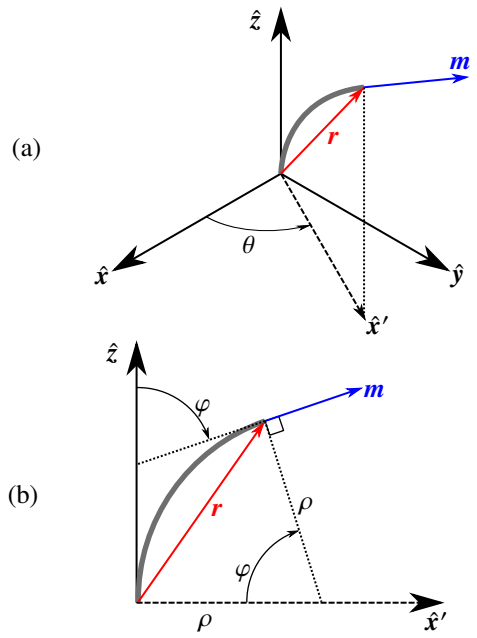

FIG. 2: A constant curvature model of a continuum robot segment with a magnet embedded in the tip with tangential magnetization.

The dipole moment of the magnet can be expressed as $\mathbf{m} = m\hat{\mathbf{m}}$, where

$$\hat{\mathbf{m}} = \begin{bmatrix} \cos\theta \sin\varphi \\ \sin\theta \sin\varphi \\ \cos\varphi \end{bmatrix}\,, \tag{4}$$

is a unit vector describing the orientation of the magnet and

$$m = MV \tag{5}$$

is the dipole magnitude, where M is the volume magnetization and V is the magnetic volume.

The magnetic field $\mathbf{b}$ produced by a magnetic dipole $\mathbf{m} = m\hat{\mathbf{m}}$ at a position $\mathbf{r} = r\hat{\mathbf{r}}$ relative to the dipole is

$$\mathbf{b} = \frac{\mu_0 m}{4\pi r^3}\left(3\hat{\mathbf{r}}\hat{\mathbf{r}}^\intercal - I\right)\hat{\mathbf{m}}\,, \tag{6}$$

where μ_0 is the magnetic permeability of free space and I is a 3×3 identity matrix [3]. The dipole field is symmetric about the dipole position, i.e. $\mathbf{b}(\mathbf{r}) = \mathbf{b}(-\mathbf{r})$, so it makes no difference if $\mathbf{r}$ is the vector from a point in space to the dipole or from the dipole to a point in space.

Inserting (2), (3), and (4) into (6) and using trigonometric identities to simplify the expression yields:

$$\mathbf{b} = \frac{\mu_0 m\varphi^3}{64\pi L^3 \sin^3(\varphi/2)} \begin{bmatrix} \sin\varphi\cos\theta \\ \sin\varphi\sin\theta \\ \cos\varphi + 3 \end{bmatrix}\,. \tag{7}$$

If the azimuth angle of the measured field is defined as

$$\alpha = \operatorname{atan}_2(b_y, b_x)\,, \tag{8}$$

then from (7) it can be seen that

$$\alpha = \theta\,, \tag{9}$$

that is, the azimuth angle of the measured field is simply equal to the azimuth angle of the bending plane.

A. Determining Deflection from the Field Polar Angle

Determining the deflection angle φ from the field measurement is more complicated. One approach is to use the polar angle of the measured magnetic field. The polar angle of the measured magnetic field can be determined using

$$\beta = \operatorname{atan}_2\left(\sqrt{b_x^2 + b_y^2}, b_z\right) = \operatorname{atan}_2(b_{x'}, b_z)\,. \tag{10}$$

The relationship between the polar angle of the field and the deflection angle of the segment can be derived by inserting (7) into (10):

$$\tan\beta = \frac{\sin\varphi}{3 + \cos\varphi}\,. \tag{11}$$

The sensitivity of β as a measure of φ is

$$\frac{\partial\beta}{\partial\varphi} = \frac{3\cos\varphi + 1}{6\cos\varphi + 10}\,, \tag{12}$$

The relationship between β and φ and its sensitivity are shown in Fig. 3.

If the bending segment is expected to experience only small deflections, a reasonable approximation of φ can be derived using the small angle identities $\sin\varphi \approx \varphi$ and $\cos\varphi \approx 1$:

$$\varphi \approx 4\tan\beta\,. \tag{13}$$

Despite the use of the small angle identities, this approximation is surprisingly accurate for moderate deflections, producing a theoretical relative error of less than 6% for $\varphi \in [0, \pi/3]$.

A more precise estimate of φ can be determined by solving (11) for φ. However, as can be seen from Fig. 3(a), the function $\beta = f(\varphi)$ is not invertible over the entire range of $\varphi \in [0, \pi]$. This results in two solutions for φ:

$$\varphi_1 = \beta - \pi/2 + \arccos\left(-3\sin\beta\right)\,,\ \varphi \in [0, \varphi_o[\tag{14}$$

$$\varphi_2 = \beta + 3\pi/2 - \arccos\left(-3\sin\beta\right)\,,\ \varphi \in]\varphi_o, \pi] \tag{15}$$

where $\varphi_o = \arccos(-1/3) \approx 0.61\pi$.

From Fig. 3, it can be seen that the sensitivity of β decreases as φ approaches φ_o, so estimates of φ from β will be more susceptible to noise in the neighbourhood of φ_o. The loss of sensitivity around φ_o and the multiple solutions for φ over large deflections are the two major downsides of using β to estimate the segment deflection. On the other hand, this approach has good sensitivity for both small and large deflections, and a direct analytical solution exists for φ. Furthermore, for small deflections the small angle approximation provides a simple and convenient means of estimating φ from β.

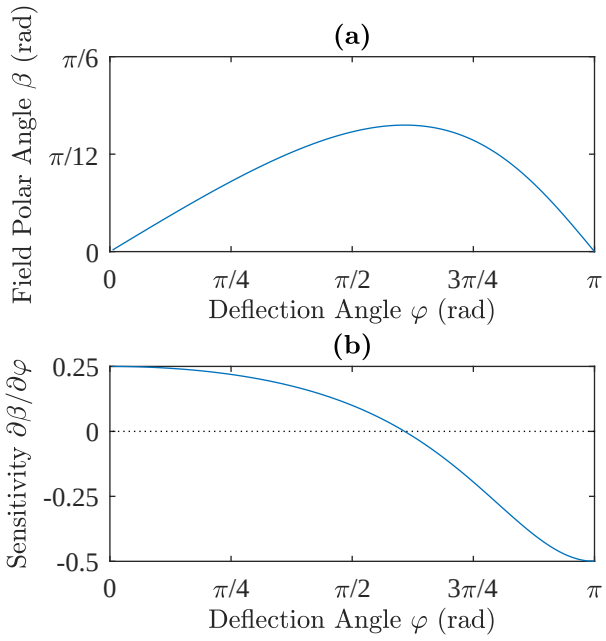

FIG. 3: (a) Polar angle β of the magnetic field vs. deflection angle φ of the robot. (b) Sensitivity of β to changes in φ.

B. Determining Deflection from the Field Magnitude

Another approach to determining segment deflection is to use the magnitude of the measured magnetic field. The measured field magnitude can be determined using

$$b = \sqrt{b_x^2 + b_y^2 + b_z^2}\,. \tag{16}$$

The relationship between the field magnitude and the deflection angle of the segment can be determined by inserting (7) into (16):

$$b = \frac{\mu_0 m \varphi^3}{64\pi L^3 \sin^3(\varphi/2)}\sqrt{6\cos\varphi + 10} \tag{17}$$

Let the normalized field magnitude $\bar{b} = \pi L^3 b/\mu_0 m$ represent the magnitude of the measured magnetic field independent of the scale of the robot, such that

$$\bar{b} = \frac{\varphi^3\sqrt{6\cos\varphi + 10}}{64\sin^3(\varphi/2)}\,. \tag{18}$$

The sensitivity of $\bar{b}$ as a measure of φ is

$$\frac{\partial\bar{b}}{\partial\varphi} = \frac{3\varphi^2 s_{\varphi/2}\left(6c_\varphi + 10\right)}{64 s_{\varphi/2}^4\sqrt{6c_\varphi + 10}} - \frac{3\varphi^3\left(s_\varphi s_{\varphi/2} + \left(3c_\varphi + 5\right)c_{\varphi/2}\right)}{64 s_{\varphi/2}^4\sqrt{6c_\varphi + 10}} \tag{19}$$

The relationship between $\bar{b}$ and φ and its sensitivity are shown in Fig. 3.

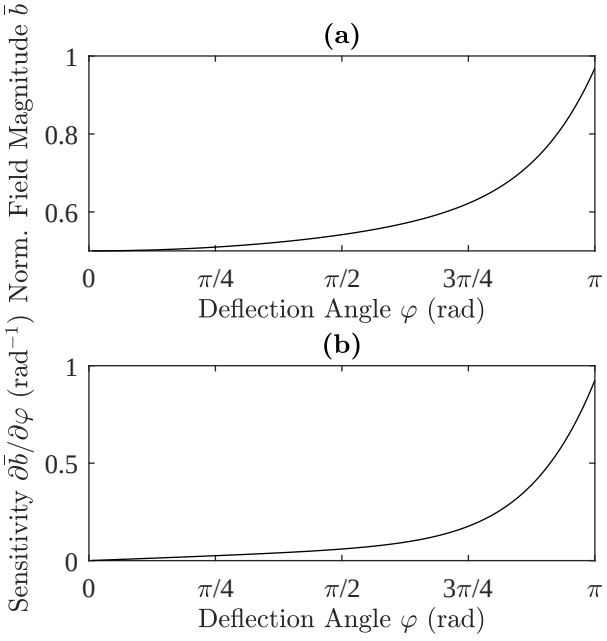

FIG. 4: (a) Normalized magnitude $\bar{b}$ of the magnetic field vs. deflection angle φ of the robot. (b) Sensitivity of $\bar{b}$ to changes in φ.

Unlike the field polar angle, the field magnitude as a function of the deflection angle is invertible over the range $\varphi \in]0, \pi]$. However, the present authors were unable to find a closed form solution to the inverse of the transcendental function (18), so numerical methods will be necessary to find φ given a measurement of b.

As can be seen in Fig. 4, the sensitivity of the field magnitude to changes in the deflection angle is poor at very small deflections and increases with larger deflections.

C. Derivation for the Magnetic Field in Terms of the Azimuth and Deflection Angles

Let $\gamma = \varphi/2$. Also, let the following compact notation for trigonometric functions be used: $c_x = \cos x$, $s_x = \sin x$. Inserting (2) and (4) into (6) yields

$$\mathbf{b} = \frac{\mu_0 m}{4\pi r^3} \begin{bmatrix} 3c_\theta^2 s_\gamma^2 - 1 & 3c_\theta s_\theta s_\gamma^2 & 3c_\theta c_\gamma s_\gamma \\ 3c_\theta s_\theta s_\gamma^2 & 3s_\theta^2 s_\gamma^2 - 1 & 3s_\theta c_\gamma s_\gamma \\ 3c_\theta c_\gamma s_\gamma & 3s_\theta c_\gamma s_\gamma & 3c_\gamma^2 - 1 \end{bmatrix} \begin{bmatrix} c_\theta s_\varphi \\ s_\theta s_\varphi \\ c_\varphi \end{bmatrix} .$$

Performing the matrix multiplication and collecting like terms yields:

$$\mathbf{b} = \frac{\mu_0 m}{4\pi r^3} \begin{bmatrix} \left((3c_\gamma s_\gamma)c_\varphi + (3c_\theta^2 s_\gamma^2 + 3s_\theta^2 s_\gamma^2 - 1)s_\varphi\right) c_\theta \\ \left((3c_\gamma s_\gamma)c_\varphi + (3c_\theta^2 s_\gamma^2 + 3s_\theta^2 s_\gamma^2 - 1)s_\varphi\right) s_\theta \\ (3c_\gamma^2 - 1)c_\varphi + (3c_\theta^2 c_\gamma s_\gamma + 3s_\theta^2 c_\gamma s_\gamma)s_\varphi \end{bmatrix} .$$

Using the trigonometric identity $s_x^2 + c_x^2 = 1$ the expression simplifies to

$$\mathbf{b} = \frac{\mu_0 m}{4\pi r^3} \begin{bmatrix} \left((3c_\gamma s_\gamma)c_\varphi + (3s_\gamma^2 - 1)s_\varphi\right) c_\theta \\ \left((3c_\gamma s_\gamma)c_\varphi + (3s_\gamma^2 - 1)s_\varphi\right) s_\theta \\ (3c_\gamma^2 - 1)c_\varphi + 3c_\gamma s_\gamma s_\varphi \end{bmatrix} .$$

Using the trigonometric identities $s_{2x}/2 = c_x s_x$ and $s_{x/2}^2 = (1 - c_x)/2$ can further simplify the expression:

$$\mathbf{b} = \frac{\mu_0 m}{8\pi r^3} \begin{bmatrix} s_\varphi c_\theta \\ s_\varphi s_\theta \\ c_\varphi + 3 \end{bmatrix} .$$

Finally, inserting (3) yields the final expression for the measured magnetic field in terms of the θ and φ:

$$\mathbf{b} = \frac{\mu_0 m \varphi^3}{64\pi s^3 \sin^3(\varphi/2)} \begin{bmatrix} s_\varphi c_\theta \\ s_\varphi s_\theta \\ c_\varphi + 3 \end{bmatrix} . \tag{20}$$

D. Uncertainty Analysis

The two methods of estimating deflection can be compared based on the level of uncertainty. Both methods rely on 3-axis field measurements from a magnetometer. Assuming a similar level of total uncertainty exists in all three axes, $\Delta b_x = \Delta b_y = \Delta b_z = \Delta b$, the uncertainty in the estimated value can be estimated with the partial derivatives:

$$\Delta\varphi_{1,\beta} = \Delta b \frac{\partial \varphi_1}{\partial \beta} \sqrt{\left(\frac{\partial \beta}{\partial b_x}\right)^2 + \left(\frac{\partial \beta}{\partial b_y}\right)^2 + \left(\frac{\partial \beta}{\partial b_z}\right)^2} \tag{21}$$

$$\Delta\varphi_{2,\beta} = \Delta b \frac{\partial \varphi_2}{\partial \beta} \sqrt{\left(\frac{\partial \beta}{\partial b_x}\right)^2 + \left(\frac{\partial \beta}{\partial b_y}\right)^2 + \left(\frac{\partial \beta}{\partial b_z}\right)^2} \tag{22}$$

$$\Delta\varphi_b = \Delta b \frac{\partial \varphi}{\partial b} \sqrt{\left(\frac{\partial b}{\partial b_x}\right)^2 + \left(\frac{\partial b}{\partial b_y}\right)^2 + \left(\frac{\partial b}{\partial b_z}\right)^2} \tag{23}$$

Even if we are lacking a direct solution for $\varphi(b)$, the partial derivative $\frac{\partial \varphi}{\partial b}$ can be computed using the reciprocal of the sensitivity of b with respect to φ:

$$\frac{\partial \varphi}{\partial b} = \left(\frac{\partial b}{\partial \varphi}\right)^{-1} . \tag{24}$$

E. Considering Z-offset

Often, it is not possible to have the sensor taking readings exactly from the point at which the robot curvature begins. There is a likelihood of the sensor measuring values at some distance along the axis from this point.

Let the sensor be located at some position $\mathbf{r}_s$ that is not at the origin of the coordinate system shown in Fig. 2. The position of the dipole relative to the sensor becomes:

$$\mathbf{r} = \mathbf{r}_m - \mathbf{r}_s , \tag{25}$$

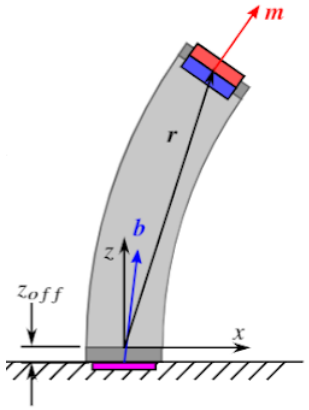

FIG. 5: Z-offset displayed in a robot segment along the axis

where $\mathbf{r}_m$ can be determined from (2) and (3), and

$$\mathbf{r}_s = \begin{bmatrix} x_s \\ y_s \\ z_s \end{bmatrix} .$$

In most cases it will be practical to ensure that $x_s = 0$ and $y_s = 0$, but if the robot design has a central backbone it may not be possible to eliminate z_s. This sensor z-offset z_s can have a significant impact on the measured field compared to the ideal case described by (7), and there is no longer an expression for b or β with respect to φ that is simple enough to be useful for direct solutions. It is still possible to model the expected field measurement by inserting (25) into (6), but numerical methods will be necessary for determining φ from a given field measurement.

III. EXPERIMENTS

A. Sensor Calibration

The sensor used in our experiments was the **Adafruit LIS3MDL Triple-Axis Magnetometer**. The manufacturer-provided values for the uncertainty, sensor noise, and the non-linearity were insignificant to cause issues with the results of the experiment. However, after repeated experiments of calculating the bending angles from the field measurements, the errors in the experiment were significant and could not be removed with reducing uncertainties in the experimental setup. This indicated the necessity to have a calibration of the sensors with an accurate field measurement device.

For this, a setup was developed that would enable us to fix a magnet with a known value of magnitude and direction of magnetization at fixed distances from a calibrated gaussmeter probe with known lengths. The magnet is fixed at 9 different distances along the axis of the gaussmeter probe. The magnet is fixed in three different orientations, with the direction of magnetization pointing in the direction of each of the three sensors of the three-axis gaussmeter. This ensures the calibration of each of the sensors independently. The direction of magnetization being along the direction of the sensor ensures that the values of the reading are significantly larger than the Earth's magnetic field, hence ensuring that fluctuations in the Earth's field have a negligible effect on the final values.

The gaussmeter is then replaced with the magnetometer, and the experiment is repeated with the same values of distance and orientation. A graph is plotted with the magnetometer readings on the y-axis and the corresponding gaussmeter values on the x-axis. A best fit line is plotted through these data points and the relationship between the two is obtained. This exercise is repeated for each directional sensor independently.

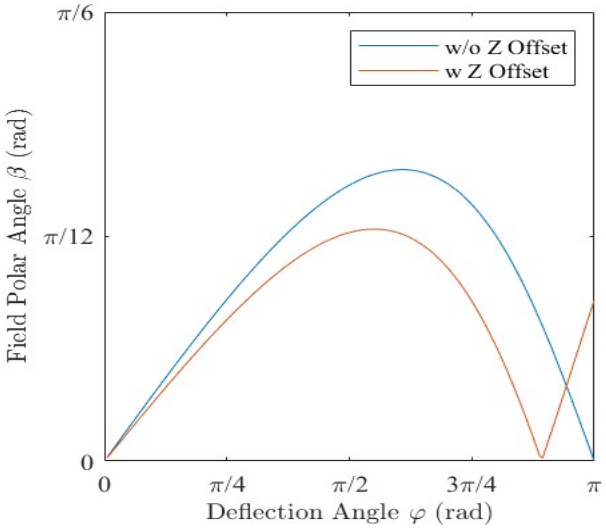

(a)

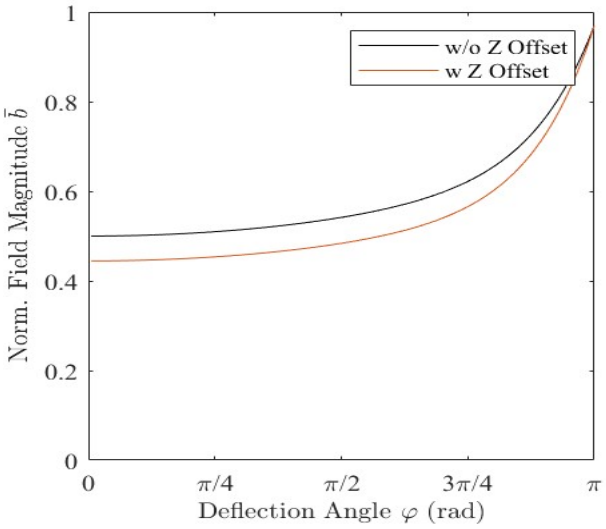

(b)

FIG. 6: Comparison of the 0 offset case with a z-offset of 3mm, for: (a) Field Polar Angle vs Deflection Angle φ (b) Normalized magnitude $\bar{b}$ of the magnetic field vs. deflection angle φ of the robot.

B. Compensation of Earth's Field

From the analytical model, we know that the angles can be determined by an accurate determination of the angles and magnitudes of the field produced by the magnet present at the tip of the continuum robot segment alone. External fields, which majorly include the effect of the Earth's magnetic field need to be eliminated once readings have been taken.
From the sensor calibration experiments, it was observed that different sensors would give wildly different relations

with the gaussmeter readings. In this situation, using a different sensor for measuring the Earth's field in the absence of the magnet, and then performing the experiment would be tedious as it would involve calibrating both the sensors and could also lead to the propagation of larger errors. Further, keeping the single sensor detachable is not ideal, as we would prefer having a single component system to keep the claim of an "embedded" system valid.

Assuming that the magnetization of the magnet is exactly along the axis of the robot segment, we know that the number of variables are only 4, namely, the Earth's field in the three mutually perpendicular directions, and the magnet field along the axis. Hence, potentially, there is a possibility of arriving at the values by performing matrix manipulations on the sensor readings in two mutually perpendicular orientations of the robot segment.

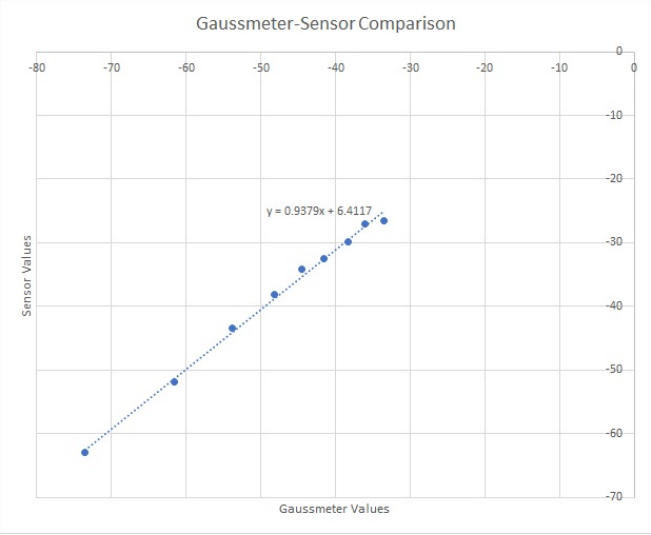

FIG. 7: Magnetometer vs Gaussmeter plots with the best fit line

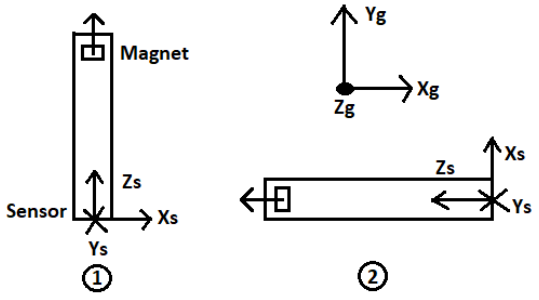

FIG. 8: Compensation method

Consider Fig. 8, in which we take sensor readings in two mutually perpendicular directions. Note here that we have two reference frames, the ground reference frame, and the sensor reference frame. To distinguish between the two, ${}^{s}b$ indicates field in the sensor reference frame and ${}^{g}b$ indicates field in the ground reference frame. With this, we know that-

$$\mathbf{b_s} = \mathbf{b_m} + \mathbf{b_e}$$

$$\mathbf{{}^{s}b_s} = \mathbf{{}^{s}b_m} + \mathbf{{}^{s}b_e}$$

When there is no deflection, we assume magnetization is along the axis:

$$\mathbf{{}^{s}b_m} = \begin{bmatrix} 0 & 0 & b_m \end{bmatrix}^T$$

In position 1, we have-

$$\mathbf{{}^{s}b_e} = \begin{bmatrix} {}^{g}b_{ex} \\ -{}^{g}b_{ez} \\ {}^{g}b_{ey} \end{bmatrix} = \begin{bmatrix} 1 & 0 & 0 \\ 0 & 0 & -1 \\ 0 & 1 & 0 \end{bmatrix} \begin{bmatrix} {}^{g}b_{ex} \\ {}^{g}b_{ey} \\ {}^{g}b_{ez} \end{bmatrix}$$

And in position 2, we have-

$$\mathbf{{}^{s}b_e} = \begin{bmatrix} {}^{g}b_{ey} \\ -{}^{g}b_{ez} \\ -{}^{g}b_{ex} \end{bmatrix} = \begin{bmatrix} 0 & 1 & 0 \\ 0 & 0 & -1 \\ -1 & 0 & 0 \end{bmatrix} \begin{bmatrix} {}^{g}b_{ex} \\ {}^{g}b_{ey} \\ {}^{g}b_{ez} \end{bmatrix}$$

Combining the two sensor readings and eliminating the redundant rows, we get-

$$\begin{bmatrix} 1 & 0 & 0 & 0 \\ 0 & 0 & -1 & 0 \\ 0 & 1 & 0 & 1 \\ 0 & 1 & 0 & 0 \end{bmatrix} \begin{bmatrix} {}^{g}b_{ex} \\ {}^{g}b_{ey} \\ {}^{g}b_{ez} \\ b_m \end{bmatrix} = \begin{bmatrix} b_{sx1} \\ b_{sy1} \\ b_{sz1} \\ b_{sx2} \end{bmatrix}$$

Here, b_{x1} denotes the sensor reading in the x direction of the sensor reference frame in position 1, and so on.

We observe that the constant matrix on the LHS is invertible, hence we can obtain the Earth's magnetic field from the two sets of sensor readings from the following equation

$$\begin{bmatrix} {}^{g}b_{ex} \\ {}^{g}b_{ey} \\ {}^{g}b_{ez} \\ b_m \end{bmatrix} = \begin{bmatrix} 1 & 0 & 0 & 0 \\ 0 & 0 & 0 & 1 \\ 0 & -1 & 0 & 0 \\ 0 & 0 & 1 & -1 \end{bmatrix} \begin{bmatrix} b_{sx1} \\ b_{sy1} \\ b_{sz1} \\ b_{sx2} \end{bmatrix}$$

The experimental setup enabled the fixing of the robot segment in mutually perpendicular positions. The validity of this method was tested out by comparing the calculated values of the Earth's magnetic field with the values obtained by detaching the same sensor from the segment and taking measurements without any magnet present in the vicinity. The results had a maximum absolute error of 5.6%, hence, validating this method.

C. Bending Angle Evaluation

After calibrating the sensor and evaluating the Earth's magnetic field using the compensation method as described in the previous subsection, we finally look at the evaluative experiments, in which the robot segment is fixed at known bending angles and the experimental bending values are determined from the analytical model displayed in section II.

Fig. 9 displays the experimental setup used for performing the experiment. It consists of the robot segment with the embedded shape sensing system which we want to validate, the experimental board, which is used to fix the aforementioned segment in fixed, known bending angles, and the top and base caps which are used in the fixing of the segment on the experimental board. To provide a clearer picture, Fig. 10 displays the entire setup for the robot segment fixed at 90° bending angle, and includes the sensor and the Arduino Uno board with the interface for connecting to a PC for processing the readings from the sensor.

We now discuss the step-by-step methodology to calculate the bending angles.

- Assemble the setup, which includes fitting the sensor onto the base of the robot segment, attaching the top cap and bottom cap to the top and bottom of the segment respectively, and connecting the Arduino Uno to the PC. The code for getting the raw data is then programmed onto the board.
- Clamp the experimental board onto the table to ensure that the directions remain fixed throughout the course of the experiment.
- Make sure the same configuration as Fig. 8 is followed while clamping (the slots on the experimental board should allow us to fix the robot segment straight and to the left). Make sure all the steps are according to this configuration, when the setup, as kept on the table, is viewed from the top.
- Fix the top cap and bottom cap into the slots as shown in Fig. 10, starting from 0° angle and then moving onto the rest. Also take the readings for the compensation method, which has slots in the experimental board for the same.
- Begin to take the readings from Tools, Serial Monitor. Allow the readings to run for some time, then de-select Autoscroll and copy-paste 1000 or so lines from the serial monitor onto a notepad file. Save this in a folder with the name as angle_value.csv (e.g. 30.csv).
- Once all readings are taken, run the code for compensate.m, this will give you the values of the Earth's magnetic field as calculated from the compensation method.
- Take note of the directions on the sensor for each of the three magnetometer axes and appropriately add/subtract the Earth's magnetic field from the final field values by changing the terms in the file named final.m
- Run final.m starting from 0.csv (change the import-data file names) and till the last angle file that has been saved. After each run, note down the values of beta and mag, which correspond to the field polar angle and the magnitude of the field.
- Modify the noted values in the respective arrays in the file testing_analytical_model_zoffset.m, and run the file to get a plot of the theoretical (with and without the appropriate offset) and the experimental values for comparison. The experiment is now complete.

IV. RESULTS

Experiments were performed to test the embedded system and to compare it with the analytical model. However, in spite of multiple iterations with several changes

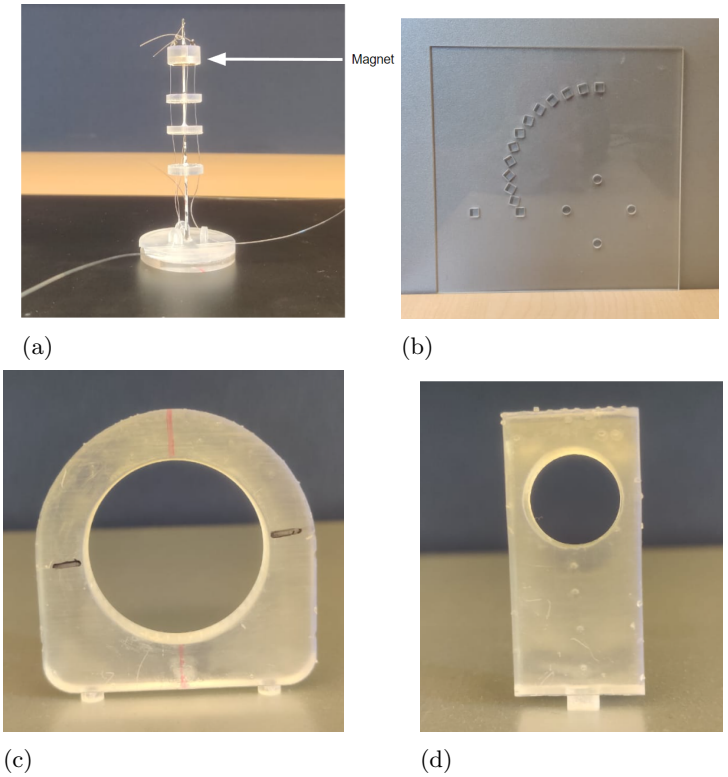

FIG. 9: a) Continuum robot segment with embedded shape sensing system, b) Experimental Board, c) Base Cap, d) Top Cap

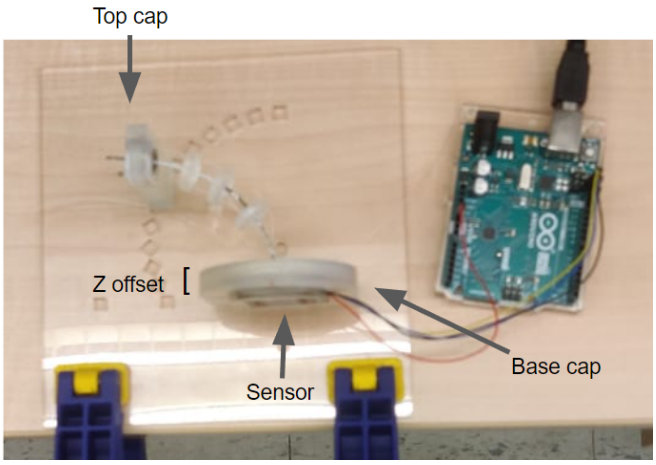

FIG. 10: Robot fixed at 90° bending angle

made in the experimental setup, there were significant errors obtained without solutions. Here, the description of the steps taken and the effect on the results are highlighted in chronological order. Some results are displayed in Fig. 11

1. The first experiment yielded results that showed results in which both the field polar angle and the field magnitude had values less than the theoretical.

2. Improvement in the setup by improving tolerances (reducing hole size to reduce wiggle, etc) did not show significant improvement in the results. This implied that the issue was in the model rather than due to system uncertainty.

3. The effect of the z-offset was investigated. The consideration of the z-offset in the model made the experimental readings agree with the theoretical values. However, there were still large differences in the field polar angle.

4. The sensor was fixed in different orientations to investigate the possibility of a disparity between the readings of the three different directional sensors. Curious results were obtained but any conclusions regarding these results were dismissed later.

5. A different sensor of the same manufacturing and model was used to perform the experiment. Surprisingly, largely different results were obtained that now made even the field magnitude values disagree with the analytical model. The use of the third sensor confirmed this discovery.

6. A well calibrated and accurate Gaussmeter was used to calibrate the three sensors, and it showed that all of them had different linear relations with the Gaussmeter readings.

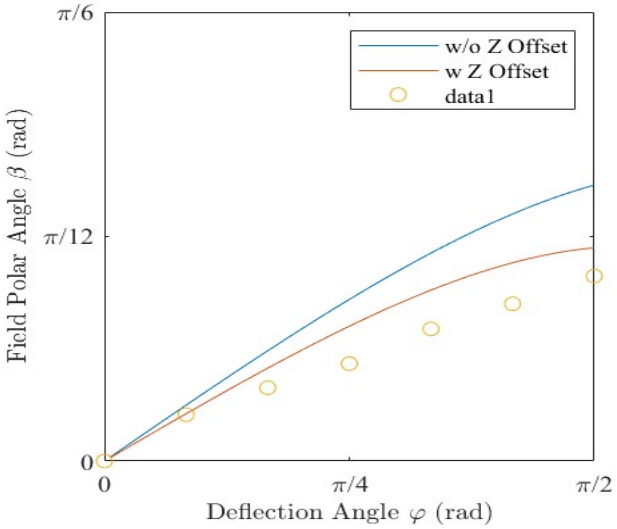

(a)

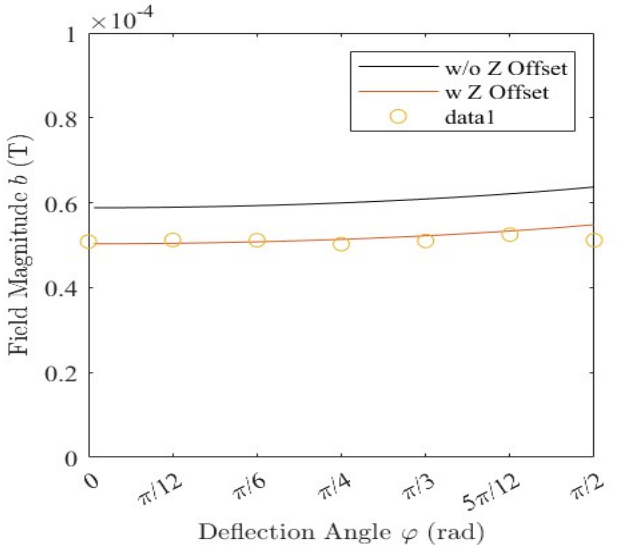

(b)

FIG. 11: Comparison of the analytical model with and without offset with the experimental results for: (a) Field Polar Angle vs Deflection Angle φ (b) Magnitude b of the magnetic field vs. deflection angle φ of the robot.

7. The calibrated sensor was used to run the experiment. Now, the field magnitude values agreed again, but the polar angles were now found to be larger than the analytical model.

8. The possibility of NiTi wire, which was used as the central backbone for the robot segment, having become axially magnetized was considered. For this, the segment was dismantled and only the top disc of the segment with the magnet and the base disc

were fixed to the experimental setup to simulate the experiment in the absence of Ni-Ti. The results now seemed to improve, but still had errors.

9. Better caps and discs were 3-D printed and the sensor was attached to the base in a more reliable way. The experiment now yielded accurate results.

10. Repeating the same experiment with the same setup without any improvements did not give repeatable results with the previous iteration. Large errors were again observed. Experimentation came to a halt after this.

V. CONCLUSIONS AND FUTURE WORK

Till the end, it was difficult to isolate the exact source of the error and to eliminate it. Here, a few possible theories regarding the errors and solutions for the same are proposed.

1. Angular uncertainty was not quantified. I.e., within the uncertainty range of the setup, what is the corresponding range of field polar angles, and from there, the bending angles. Possible solutions could include using a different parameter other than the field polar angle and magnitude that has a low sensitivity with respect to the above terms.

2. Better tolerances in the setup. Even after the improvements, there was still a wiggle present and it was difficult to ensure that each of the caps lay perfectly horizontal on the experimental board. Further, the sensor itself was not fixed in place since it was temporarily attached using only tape. Better manufacturing or other techniques to limit the uncertainty should be investigated.

3. Real time sensing with demonstrable capabilities and 3D shape estimation with ground truth values being provided by a set of cameras was considered as future work after the errors had been eliminated.

[1] H. Guo, F. Ju, Y. Cao, F. Qi, D. Bai, Y. Wang, and B. Chen, Continuum robot shape estimation using permanent magnets and magnetic sensors, Sensors and Actuators, A: Physical **285**, 519 (2019).

[2] S. K. Sahu, C. Sozer, B. Rosa, I. Tamadon, P. Renaud, and A. Menciassi, Shape Reconstruction Processes for Interventional Application Devices: State of the Art, Progress, and Future Directions, Frontiers in Robotics and AI **8**, 758411(1 (2021).

[3] J. J. Abbott, E. Diller, and A. J. Petruska, Magnetic Methods in Robotics, Annu. Rev. Control. Robot. Auton. Syst. **3**, 57 (2020).